PHILOSOPHICAL TRANSACTIONS A

rsta.royalsocietypublishing.org

Research

Article submitted to journal

Subject Areas:
Computational biology, Computer modelling and simulations, Medical computing

Keywords:
computational methods, tumor heterogeneity, Fisher-Kolmogorov

Author for correspondence:
Hector Gomez
e-mail: hectorgomez@purdue.edu

THE ROYAL SOCIETY PUBLISHING

How heterogeneity drives tumor growth: A computational study

Hector Gomez[1,2,3]

[1]School of Mechanical Engineering, Purdue University, West Lafayette, IN, USA.
[2]Weldon School of Biomedical Engineering, Purdue University, West Lafayette, IN, USA.
[3]Purdue Center for Cancer Research, Purdue University, West Lafayette, IN, USA.

Although cancerous tumors usually originate from a single cell, they normally evolve into a remarkably heterogeneous agglomeration of cells. Heterogeneity is a pervasive and almost universal feature of tumors, but its origin and consequences remain poorly understood. Tumor heterogeneity has been usually associated with poor prognosis, but a better understanding of it may lead to more personalized diagnosis and therapy. Here, we study tumor heterogeneity developing a computational model in which different cell subpopulations compete for space. The model suggests that aggressive tumor subpopulations may become even more aggressive when they grow with a non-aggressive subpopulation. The model also provides a mechanistic explanation of how heterogeneity drives growth. In particular, we observed that even a mild heterogeneity in the proliferation rates of different cell subpopulations leads to a much faster overall tumor growth when compared to a homogeneous tumor. The proposed model may be a starting point to study tumor heterogeneity computationally and to suggest new hypotheses to be tested experimentally.

1. Introduction

Tumor heterogeneity has been systematically observed for over five decades and is recognized to have profound clinical consequences for disease diagnosis and therapy design. Heterogeneity manifests itself at multiple levels [1,2]. For example, tumors are different from patient to patient even if the cancer type is nominally the same. This kind of variability, known as inter-tumor heterogeneity,

may have a genetic origin, but can also be caused by other factors. Indeed, recent research has shown that differences in the tumor's microenvironment — non-malignant cells, molecules and vessels that surround the tumor — can also drive inter-tumor heterogeneity [3]. Another major type of heterogeneity is related to the tumor's progression. This refers to the variability of a single tumor on a single patient as time evolves. The idea of tumor progression was first highlighted by Foulds [4] and has been often used to explain the development of tumor drug resistance. Although inter-tumor heterogeneity and tumor progression are very important for cancer research, here we focus on a third type of heterogeneity, namely, intra-tumor heterogeneity [5]. This refers to differences within a single tumor at one point in time. Because this is the focus of the paper, we will simply use the word heterogeneity to refer to intra-tumor heterogeneity. The differences between the cells of a tumor, can relate to their morphology [6], phenotype [7], DNA [8,9] and other aspects, including microenvironmental factors [10–12]. Although there is a lot of direct evidence showing that tumors are a remarkably heterogeneous cluster of cells, the origin and consequences of this variability are not well understood [13]. Usual examples of the importance of tumor heterogeneity include the failure of drugs that are effective only against a specific cell subpopulation of the tumor, or misleading evaluation of the tumor severity because the biopsy missed an aggressive cell type. Tumor heterogeneity is usually explained by the existence of multiple clonal subpopulations within a single tumor [7]. Those subpopulations will have different properties, including proliferation rates and motile capacities.

Here, we study tumor heterogeneity by using a computational model in which multiple clonal subpopulations compete for space. When applied to a homogeneous tumor, the model becomes the Fisher-Kolmogorov equation, a classical tumor-growth model that has been widely used to model brain [14–16] and breast [17,18] cancer. The model suggests that an aggressive cell subpopulation can become even more aggressive if it grows in combination with a non-aggressive cell type. The model also predicts that even a mild heterogeneity in the growth rate of different subpopulations can lead to a dramatic increase in the overall growth of the tumor, providing a potential mechanism to explain how heterogeneity drives growth. We believe that the model can be used to understand the role of heterogeneity in tumor growth and to design better therapies.

2. Model of intra-tumoral heterogeneity

(a) Model derivation

We consider a tumor composed of N_c clonal subpopulations. We call ρ_i the cellular density (number of cells per unit volume) of the i-th clone where i takes values from 1 to N_c. The motility of the tumor cells of the i-th clone is represented by the constant D_i and their proliferation by g_i. The system of partial differential equations that controls the dynamics of the tumor is assumed to be

$$\frac{\partial \rho_i}{\partial t} = D_i \Delta \rho_i + g_i \rho_i \left(1 - \sum_{i=1}^{N_c} \rho_i / k\right); \quad i = 1, \ldots, N_c \tag{2.1}$$

where k is a constant parameter referred to as carrying capacity [19]. The carrying capacity is a tissue property that represents the maximum cellular density for which additional cell proliferation is favored. Thus, the last term in parentheses on the right hand side of Eq. (2.1) can be interpreted as a measure of the available space in the tissue for cell proliferation. This term is key in the model because it couples all the unknowns in the system. Note that we refer to the tumor represented by Eq. (2.1) as heterogeneous because the proliferation rate and the cell motility properties vary among different subpopulations of the tumor, not because they are functions of space. The g_i's and the D_i's are constants. Notice that this is in contrast with [20] where the authors study intra-tumor heterogeneity taking a carrying capacity that varies in space.

To gain further insight into the dynamics of the system, we define $\rho = \sum_{i=1}^{N_c} \rho_i$. If we apply Eq. (2.1) to a homogeneous tumor with $D_i = D$ and $g_i = g$ for all $i = 1, \ldots, N_c$, we would wish to

retrieve a well-established model for homogeneous tumor growth. Summing all the equations in (2.1), we obtain a relation for $\rho = \sum_{i=1}^{N_c} \rho_i$ that defines the overall growth of the tumor as

$$\frac{\partial \rho}{\partial t} = D\Delta\rho + g\rho(1-\rho/k) \tag{2.2}$$

Eq. (2.2) is the Fisher-Kolmogorov model, which predicts logistic growth combined with diffusion-like cell migration. The Fisher-Kolmogorov model has been widely used to study brain [21–25] and breast tumors [26,27].

In contrast, if we assume homogeneous cell motility properties, i.e., $D_i = D$ for all $i = 1, \ldots, N_c$, but we allow the g_i's to be different, summing all the equations in (2.1), we get

$$\frac{\partial \rho}{\partial t} = D\Delta\rho + (1-\rho/k)\sum_{i=1}^{N_c} g_i\rho_i \tag{2.3}$$

As we will show later, the dynamics of Eq. (2.3) and Eq. (2.1) are dramatically different when the g_i's are not equal to each other, even if $\frac{1}{N_c}\sum_{i=1}^{N_c} g_i = g$. Heterogeneity in the motility properties also changes the overall growth kinetics, but to a lesser extent.

Further insight into the differences between the system (2.1) and the classical homogeneous model (2.2) can be gained studying the following situation: Let the D_i's be arbitrary constants and the proliferation rates be heterogeneous among different subpopulations. If we assume that $\frac{1}{N_c}\sum_{i=1}^{N_c} g_i = g$ and $\rho_i(t) = \rho(t)/N_c$ for all $i = 1, \ldots, N_c$ and for all t, then the dynamics of Eqns. (2.1) and (2.2) are identical. Although the condition $\rho_i(t) = \rho(t)/N_c$ is very stringent and will almost always be violated, this analysis provides a criterion to study the effect of heterogeneous proliferation rates in a way that allows for direct comparison with the homogeneous model. This criterion is given by the equation $\frac{1}{N_c}\sum_{i=1}^{N_c} g_i = g$ and will be used repeatedly in the paper.

Another quantity of interest is the total number of cancerous cells in a given region of the tissue Ω, irrespective of their spatial distribution. This can be defined as

$$C_{g_1 g_2 \ldots g_{N_c}}(t) = \int_\Omega \sum_{i=1}^{N_c} \rho_i \mathrm{d}x = \int_\Omega \rho \mathrm{d}x \tag{2.4}$$

By integrating all the equations in (2.1) on the domain Ω and summing over the clonal subpopulations, we can show that if $g_i = g$ for all $i = 1, \ldots, N_c$, then, under the assumption of flux-free boundary conditions, $C_{g_1 g_2 \ldots g_{N_c}}(t) = C_{gg\ldots g}(t)$ for all t even if the D_i's are different.

(b) Model problem

We use the following model problem to study the impact of heterogeneity on tumor growth

$$\frac{\partial \rho_i}{\partial t} = D_i\Delta\rho_i + g_i\rho_i\left(1 - \textstyle\sum_{i=1}^{N_c}\rho_i/k\right); \quad i = 1, \ldots, N_c \quad \text{in} \quad \Omega \times [0,T] \tag{2.5}$$

$$\nabla\rho_i \cdot \boldsymbol{n} = 0; \qquad i = 1, \ldots, N_c \quad \text{on} \quad \Gamma \times [0,T] \tag{2.6}$$

$$\rho_i(\boldsymbol{x}, 0) = k k_i^f \exp(-d_i(\boldsymbol{x})/\ell); \qquad i = 1, \ldots, N_c; \quad \boldsymbol{x} \in \Omega \tag{2.7}$$

where $\Omega = [0, L]^2$ is the problem domain, Γ is the boundary of Ω, $\boldsymbol{n}$ its unit outward normal and $[0, T]$ the time interval of interest. We will take $L = 250$ mm for all the simulations in the paper. The constant $\ell = 10$ mm is a measure of the initial size of the clones and $d_i(\boldsymbol{x})$ represents the Euclidean distance between the points $\boldsymbol{x}$ and $\boldsymbol{p}_i$. Here, the point $\boldsymbol{p}_i$ identifies the center of the i-th clone. The definition of the initial cellular density includes the additional parameter k_i^f, which denotes the fraction of the carrying capacity occupied by the i-th clone at the initial time. Our model problem allows us to study four types of intra-tumor heterogeneity varying the parameters g_i, D_i, $\boldsymbol{p}_i$ and k_i^f among the different clones.

(c) Computational method

We use a semi-implicit, first-order accurate time stepping scheme to perform the time discretization. We divided the time interval of interest $[0, T]$ into equal-size subintervals (t_n, t_{n+1}) where $n = 0, \ldots, N-1$, and such that $t_0 = 0$ and $t_N = T$. If we define the time step as $\Delta t = t_{n+1} - t_n$ and ρ_i^n denotes the time-discrete approximation to $\rho(\boldsymbol{x}, t_n)$, the algorithm can be written as

$$\frac{\rho_i^{n+1} - \rho_i^n}{\Delta t} = D_i \Delta \rho_i^{n+1} + g_i \rho_i^n (1 - \rho^n/k) \tag{2.8}$$

This scheme combines advantages of implicit and explicit methods. It allows to take larger time steps than explicit algorithms, but it avoids the nonlinearity of a fully-implicit method.

Eq. (2.8) can be rewritten as

$$(\boldsymbol{I}_d - \Delta t D_i \Delta)\rho_i^{n+1} = \rho_i^n + \Delta t g_i \rho_i^n (1 - \rho^n/k) \tag{2.9}$$

where $\boldsymbol{I}_d$ represents the identity operator. Note that Eq. (2.9) is still continuous in space and, thus, we are yet to perform spatial discretization. The space discretization will transform the operator $(\boldsymbol{I}_d - \Delta t D_i \Delta)$ into a matrix, which will be different for each subpopulation when the motility properties of the tumor are heterogeneous. When we use standard second-order accurate central differences on a uniform grid, we can determine analytically the eigenvalues and the eigenvectors of the matrix[1] and use the concept of fast Poisson solver, which provides an algorithm with optimal complexity; see [29,30] for more details. Here, we also approximate the right-hand side of Eq. (2.9) using direct collocation at the grid points. Listing 1, provided below, is a MATLAB® implementation of the algorithm for a problem with $N_c = 20$ subpopulations. The computations really take place in lines 19-27. The remaining lines of code define the mesh, model parameters, initial conditions and the eigenvalues of the matrix. The code executes the 1500 time steps necessary to reach a simulated time of 1.5 y in a few seconds on a regular desktop. Note that the code neither saves nor plots the solution, but those capabilities can be added straightforwardly.

Listing 1: MATLAB® code to solve the proposed model

```
1  N = 64; L = 250; dx = L/(N-1); dx2 = dx^2; x = (0:dx:L)'; [xx,yy]= meshgrid(x',x);
2  LEV = (((2*cos(pi*(0:N-1)'/(N-1)))-2)*ones(1,N)); LEV = LEV + LEV';
3  dt = 1e-3; L1 = dt/dx2; Tmax = 1.5; ntmax = round(Tmax/dt) + 1;
4
5  Nc = 20;                                          % Number of subpopulations
6  k  = 2e6; D0 = 1; Dm = 1000; g = 4.82; ell = 10; % Homogeneous parameters
7
8  ux = rand(1,Nc); ux = (2*ux-1)/10; px = (0.5+ux)*L;
9  uy = rand(1,Nc); uy = (2*uy-1)/10; py = (0.5+uy)*L;
10 kf = rand(1,Nc); sk = sum(kf); kf = .05*k*kf/sk;
11 r  = rand(1,Nc); gf = Nc*r*g/sum(r);
12 z  = rand(1,Nc); df = z/sum(z); D = D0 + Dm*df;
13
14 for i = 1:Nc; d(:,:,i)   = sqrt((xx-px(i)).^2 + (yy-py(i)).^2); end
15 for i = 1:Nc; U(:,:,i)   = kf(i)*exp(-d(:,:,i)/ell)           ; end
16 for i = 1:Nc; LHS(:,:,i) = ones(N,N) - D(i)*L1*LEV            ; end
17
18 t = 0; it = 0;
19 while it < ntmax
20  t = t+dt; it = it + 1;
21  Ut = sum(U,3);
22  for i=1:Nc
23   hatRHS(:,:,i) = dct2(U(:,:,i) + dt*gf(i)*(1-Ut(:,:)/k).*U(:,:,i));
24   hatU(:,:,i)   = hatRHS(:,:,i)./LHS(:,:,i);
25   U(:,:,i)      = idct2(hatU(:,:,i));
26  end
27 end
```

[1] If we discretize the Laplace operator using finite elements with a uniform mesh of linear triangular elements we obtain an identical matrix [28]

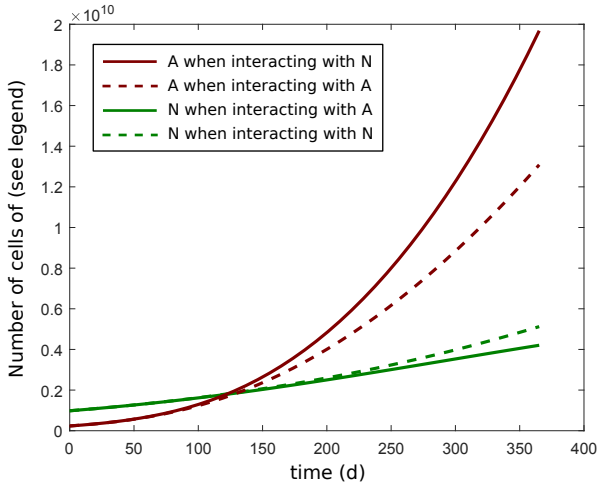

Figure 1: Growth dynamics of aggressive (A) and non-aggressive (N) cell subpopulations when interacting with each other (solid lines) or with themselves (dashed lines). The simulations were performed assuming homogeneous motility properties with $D_1 = D_2 = 50$ mm^2/y [22] and taking $k_1^f = 0.8070$, $k_2^f = 0.1930$, $u_1 = -0.0500$, $u_2 = 0.0840$, $v_1 = -0.0120$, $v_2 = 0.0680$, but the described interaction mechanism is independent of the values taken for the parameters D_i, k_i^f and $\boldsymbol{p}_i$.

3. Results

(a) Aggressive clones become more aggressive when they interact with non-aggressive subpopulations

As a first illustration of how the interaction between two different subpopulations can change the growth kinetics of the individual clones, we simulated the model problem (2.5)–(2.7) taking $N_c = 2$. The two clonal subpopulations correspond to a non-aggressive cell type (N) represented by a proliferation rate $g_N = 2.377$ y^{-1} and a more aggressive subpopulation (A) represented by $g_A = 7.263$ y^{-1}. We performed four simulations taking the parameters $g_1 = g_A$, $g_2 = g_N$ for the first one; $g_1 = g_2 = g_A$ for the second one; $g_1 = g_N$, $g_2 = g_A$ for the third one; and $g_1 = g_2 = g_N$ for the fourth one. The plot shows that an aggressive cell subpopulation grows faster when it interacts with a non-aggressive subpopulation than when it interacts with itself. Conversely, non-aggressive cells grow more slowly when they do so in combination with aggressive cells than when they interact with themselves. This simple example illustrates non-trivial interactions between subpopulations with different growth rates and can provide useful information to interpret experimental data showing that co-cultures of tumor subpopulations grow at different rates than they do when they grow by themselves [6].

(b) Heterogeneity of the proliferation rate significantly increases overall tumor growth

We will now use the model problem (2.5)–(2.7) to study how a heterogeneous proliferation rate drives growth. To model heterogeneous growth rates, and compare the growth kinetics with those of a single-clone tumor we will always use values of the g_i's that satisfy the constraint $\frac{1}{N_c}\sum_{i=1}^{N_c} g_i = g$, where g is the proliferation rate of the single-clone model. To satisfy this constraint we defined the random variable r with uniform distribution in the interval $[0, 1]$. Then,

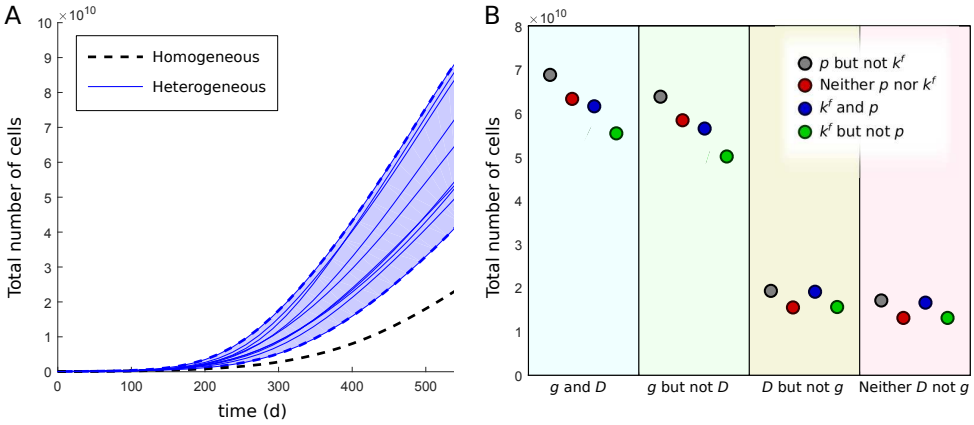

Figure 2: A. Overall growth kinetics for homogeneous and heterogeneous tumors. For the heterogeneous tumors, we present 10 simulations that correspond to 10 different sets of g_i's, all of them satisfying the constraint (3.1); B. Influence on overall tumor growth of the heterogeneity in motility properties and the initial distribution of subpopulations.

we took N_c realizations of it, obtaining the values r_i for $i = 1, \ldots, N_c$. The proliferation rates were defined as

$$g_i = gN_c \frac{r_i}{\sum_{j=1}^{N_c} r_j} \tag{3.1}$$

The proliferation rates obtained using Eq. (3.1) satisfy the constraint $\frac{1}{N_c}\sum_{i=1}^{N_c} g_i = g$ as desired.

To study the influence of heterogeneous growth rates on the overall growth of the tumor, we solved the model problem (2.5)–(2.7) for $N_c = 20$ subpopulations. We performed 11 simulations of the model problem. In 10 simulations, we determined the (heterogeneous) growth rates using Eq. (3.1), while in the remaining one, we simply took $g_i = g = 4.82$ y^{-1} for all clones, which represents a tumor with homogeneous growth rate. As shown before, the latter simulation will produce exactly the same overall tumor growth dynamics as a single-clone simulation given by Eq. (2.2) with $g = 4.82$ y^{-1}. Although we are primarily interested in heterogeneous proliferation rates in this section, we also introduce heterogeneity in the initial distribution of cells (k_i^f and $\boldsymbol{p}_i$) to represent a more realistic scenario. The parameters k_i^f and $\boldsymbol{p}_i$ were different for each clone, but their specific values (which do not affect the conclusions of this section) were kept constant throughout the 11 simulations.

Fig. 2A shows the time evolution of the total number of tumor cells $\left(\int_\Omega \rho \mathrm{d}x\right)$ for 10 simulations of heterogeneous tumors (solid blue lines) and the simulation of homogeneous tumor growth (dashed black line). In all cases, the heterogeneous tumor grows significantly faster than the homogeneous one. At $t = 1.5$ y, the total number of cells is between two- and five-fold larger for the heterogeneous tumor. The results show that heterogeneous tumors are more effective competing for space than homogeneous tumors and suggest a potential explanation of how heterogeneity drives growth and results in poorer prognosis.

(c) Heterogeneity in motility and initial distribution of subpopulations has a mild influence on the overall tumor growth

We can have a more detailed understanding of the role of intra-tumor heterogeneity on the overall tumor growth by varying the parameters g_i, $\boldsymbol{p}_i$, k_i^f and D_i simultaneously. The motility heterogeneity was defined using the expression

$$D_i = D_0 + D_m D_i^f \quad \text{where} \quad D_i^f = \frac{z_i}{\sum_{j=1}^{N_c} z_j} \tag{3.2}$$

Table 1: Deterministic parameters for the model problem

Parameter	Value
D_m	1000 $\text{mm}^2\ \text{y}^{-1}$
D_0	1 $\text{mm}^2\ \text{y}^{-1}$
g	4.82 y^{-1}

The z_i's in Eq. (3.2) are realizations of a random variable with uniform distribution in $[0, 1]$. The maximum cell density heterogeneity was modeled taking k_i^f as realizations of a uniform distribution in the interval $[0, N_c/20]$. The heterogeneity in the location of the clones was modeled taking $\boldsymbol{p}_i = \{(1/2 + u_i)L, (1/2 + v_i)L\}^T$, where u_i and v_i are realizations of a random variable with uniform distribution in $[-0.2, +0.2]$. The deterministic parameters of the model are given in Table 1. These parameters will be kept fixed for the rest of the paper.

Fig. 2B shows the results of 16 simulations, providing the total number of tumor cells at time 1.5 y for all combinations of homogeneous/heterogeneous properties. The heterogeneous parameters g_i, D_i, k_i^f and $\boldsymbol{p}_i$ were randomly generated as described before; see Eqns. (3.1)–(3.2) and the text that follows. The random parameters were generated only once, and re-used for all the simulations. The reference values for homogeneous properties were taken from Table 1. We also took $D_i^f = 1.84 \times 10^{-3}$, $u_i = v_i = 0$ for all $i = 1, \ldots, N_c$ for the simulations of homogeneous tumors. The labels in Fig. 2B indicate which properties are heterogeneous in the simulations. Consistently with Fig. 2A, we observe that heterogeneity of the growth rates among different subpopulations makes a dramatic difference in the total number of cells. We observe that when the $\boldsymbol{p}_i$'s are heterogeneous, the tumor always grows faster, but the increase in global growth is approximately twofold higher when the g_i's are also heterogeneous. Heterogeneity in the k_i^f's seems to have a negative influence in global growth, which is almost negligible for tumors with homogeneous growth rates and more significant when the growth rates are heterogeneous. Finally, heterogeneity in motility properties has a positive effect on the overall tumor growth, but in contrast with what happens with the $\boldsymbol{p}_i$'s, the effect is approximately twofold stronger when the growth rates are homogeneous.

(d) Dynamics of individual clonal subpopulations

The previous results clearly show that growth rate heterogeneity plays the most significant role in the overall tumor growth. Here, we analyze in more detail how different clones compete with each other for space. We performed two simulations with $N_c = 20$ clonal subpopulations. The cells motility properties and initial distribution of subpopulations (k_i^f and $\boldsymbol{p}_i$) were assumed to be heterogeneous. In the first simulation (shown in Fig. 3) we took $g_i = g = 4.82\ \text{y}^{-1}$ for all $i = 1, \ldots, N_c$, while in the second one (Fig. 4) we used Eq. (3.1) to define a tumor with heterogeneous growth rate. Figs. 3 and 4 are arranged identically. Panels A, B and C show snapshots of $\rho = \sum_{i=1}^{N_c} \rho_i$ at times $t = 54.75$ d, $t = 182.5$ d and $t = 365$ d, while panel D shows the time evolution of the total number of tumor cells. Panels E, F and G show the time evolution of the different subpopulations. The semitransparent colored regions represent the areas in which a particular subpopulation has a cell density larger than $k/10$. The time evolution of the number of cells for each subpopulation is represented in panels H, utilizing the same colors used in E-G. The comparison reinforces the idea that heterogeneous proliferation rates lead to significantly larger overall tumor growth. This is apparent by comparing panels C and D in Figs. 3 and 4. A comparison of panels E-H suggests that heterogeneous tumors grow through a winner-takes-all process in which the subpopulation with the highest proliferation rate would take up most of the space at long time scales. Fig. 4H shows that the subpopulation represented by $i = 2$, which happens to be the one with the largest proliferation rate, is the dominant one at the end of the

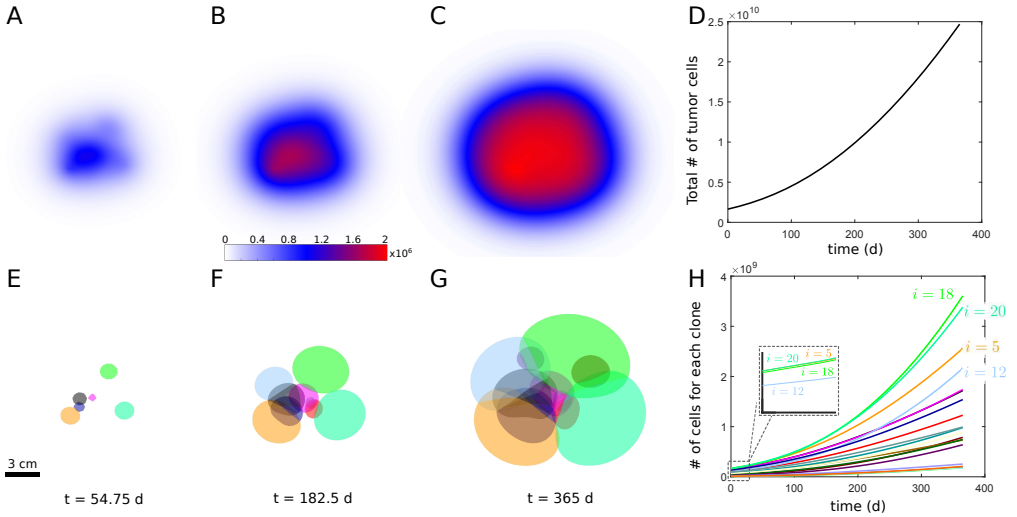

Figure 3: Growth of a tumor with $N_c = 20$ clonal subpopulations. The motility properties and initial distribution of cells are heterogeneous across different subpopulations, but the growth rates are homogeneous; A-D. Growth dynamics of the overall tumor; E-H. Dynamics of the individual subpopulations.

simulation, even though its initial cellular density was smaller than those of other subpopulations; see inset.

The situation is more complex for the homogeneous tumor; see Fig. 3H. The proliferation rates are all identical in this case, and the initial cellular density does not seem to play a critical role, either. For example, the initial cellular density of subpopulation $i = 5$ and $i = 20$ are indistinguishable (see inset), but $i = 20$ grows faster. Also, the initial cellular density of $i = 18$ is slightly lower than that of $i = 5$, but at the end of the simulation $i = 18$ is the dominant subpopulation. In the homogeneous tumor, the dominant subpopulation seems to be established in a complex manner that involves heterogeneity in the parameters k_i^f, D_i and $\boldsymbol{p}_i$ simultaneously. In particular, heterogeneity in the parameter $\boldsymbol{p}_i$ may create local differences in the available space for growth, defined mathematically as $1 - \rho/k$, which we believe produces similar results to the spatial dependence of the carrying capacity k studied in [20].

4. Discussion

Although most tumors are heterogeneous, the origin and consequences of heterogeneity remain poorly understood. This paper studies the role of heterogeneity on tumors that grow competing for space in the host tissue. Our model predicts that a tumor composed by multiple clonal subpopulations with heterogeneous growth rates will grow much faster than a homogeneous tumor. The model also indicates that an aggressive subpopulation may become even more aggressive when it grows with a non-aggressive one. Also, a non-aggressive subpopulation becomes even less aggressive when it grows with a more aggressive cell type.

We believe our model can be particularly useful to study the effect of therapy on tumor growth [31]. One of the usual limitations of cytotoxic chemotherapies when they are used to treat heterogeneous tumors is that they are effective only on some subpopulations of the tumor. Our model indicates that if we apply a therapy to a heterogeneous tumor and the drug is effective only on the less aggressive cell types, the overall effect may be detrimental for the patient in the long term because the space freed up by the killed non-aggressive cells will be eventually repopulated by more aggressive cells that grow faster.

Data Accessibility. The article has no additional data.

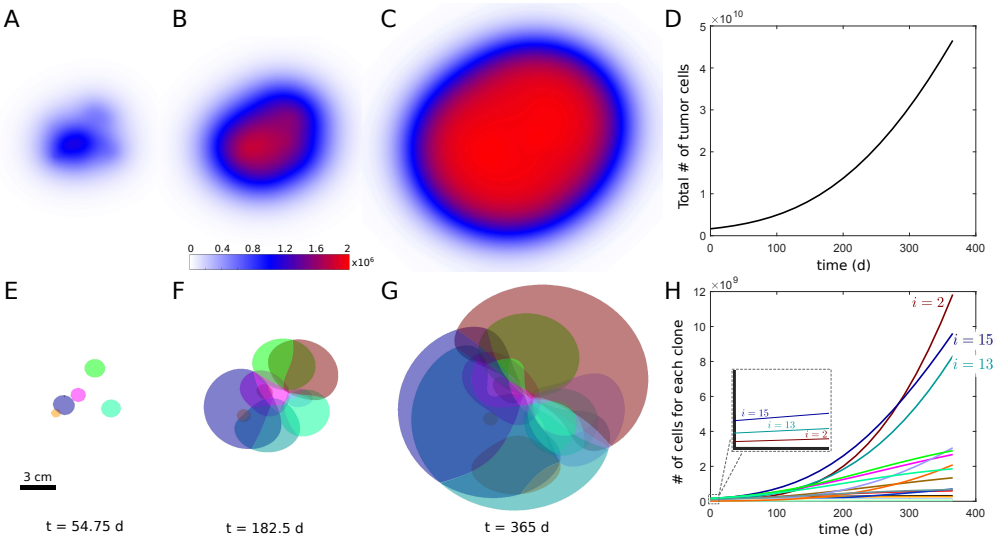

Figure 4: Growth of a tumor with $N_c = 20$ clonal subpopulations. The motility properties, proliferation rates and initial distribution of cells are heterogeneous across different subpopulations; A-D. Growth dynamics of the overall tumor; E-H. Dynamics of the individual subpopulations.

Competing Interests. The author declares that he has no competing interests.

References

1. A. Marusyk and K. Polyak, "Tumor heterogeneity: causes and consequences," *Biochimica et Biophysica Acta (BBA)-Reviews on Cancer*, vol. 1805, no. 1, pp. 105–117, 2010. (doi:10.1016/j.bbcan.2009.11.002).
2. A. Pribluda, C. Cecile, and E. L. Jackson, "Intratumoral heterogeneity: from diversity comes resistance," *Clinical Cancer Research*, vol. 21, no. 13, pp. 2916–2923, 2015. (doi:10.1158/1078-0432.CCR-14-1213).
3. C. Miething, C. Scuoppo, B. Bosbach, I. Appelmann, J. Nakitandwe, J. Ma, G. Wu, L. Lintault, M. Auer, P. K. Premsrirut, *et al.*, "PTEN action in leukaemia dictated by the tissue microenvironment," *Nature*, vol. 510, no. 7505, p. 402, 2014. (doi:10.1038/nature13239).
4. L. Foulds, *Neoplastic development*, vol. 2. Academic Press, 1975.
5. B. Y. Oh, H.-T. Shin, J. W. Yun, K.-T. Kim, J. Kim, J. S. Bae, Y. B. Cho, W. Y. Lee, S. H. Yun, Y. A. Park, *et al.*, "Intratumor heterogeneity inferred from targeted deep sequencing as a prognostic indicator," *Scientific reports*, vol. 9, no. 1, p. 4542, 2019. (doi:10.1038/s41598-019-41098-0).
6. G. H. Heppner and B. E. Miller, "Tumor heterogeneity: biological implications and therapeutic consequences," *Cancer and Metastasis Reviews*, vol. 2, no. 1, pp. 5–23, 1983. (doi:10.1007/BF00046903).
7. P. C. Nowell, "The clonal evolution of tumor cell populations," *Science*, vol. 194, no. 4260, pp. 23–28, 1976. (doi:10.1126/science.959840).
8. A. Aguilera and T. García-Muse, "Causes of genome instability," *Annual review of genetics*, vol. 47, pp. 1–32, 2013. (doi:10.1146/annurev-genet-111212-133232).
9. A. Aguilera and B. Gómez-González, "Genome instability: a mechanistic view of its causes and consequences," *Nature Reviews Genetics*, vol. 9, no. 3, p. 204, 2008. (doi:10.1038/nrg2268).

10. L. A. Liotta and E. C. Kohn, "The microenvironment of the tumour–host interface," *Nature*, vol. 411, no. 6835, p. 375, 2001. (doi:10.1038/35077241).
11. P. Friedl and S. Alexander, "Cancer invasion and the microenvironment: plasticity and reciprocity," *Cell*, vol. 147, no. 5, pp. 992–1009, 2011. (doi:10.1016/j.cell.2011.11.016).
12. A. R. Anderson, A. M. Weaver, P. T. Cummings, and V. Quaranta, "Tumor morphology and phenotypic evolution driven by selective pressure from the microenvironment," *Cell*, vol. 127, no. 5, pp. 905–915, 2006. (doi:10.1016/j.cell.2006.09.042).
13. J. West and P. K. Newton, "Cellular interactions constrain tumor growth," *Proceedings of the National Academy of Sciences*, vol. 116, no. 6, pp. 1918–1923, 2019. (doi:10.1073/pnas.1804150116).
14. H. Gomez, "Quantitative analysis of the proliferative-to-invasive transition of hypoxic glioma cells," *Integrative Biology*, vol. 9, no. 3, pp. 257–262, 2017. (doi:10.1039/c6ib00208k).
15. V. M. Pérez-García, M. Bogdanska, A. Martínez-González, J. Belmonte-Beitia, P. Schucht, and L. A. Pérez-Romasanta, "Delay effects in the response of low-grade gliomas to radiotherapy: a mathematical model and its therapeutical implications," *Mathematical Medicine and Biology*, pp. 307–329, 2015. (doi:10.1093/imammb/dqu009).
16. L. Curtin, A. Hawkins-Daarud, A. Porter, M. R. Owen, K. van der Zee, and K. R. Swanson, "Modeling the role of hypoxia in glioblastoma growth and recurrence patterns," *bioRxiv*, p. 691238, 2019.
17. A. M. Jarrett, D. A. Hormuth, S. L. Barnes, X. Feng, W. Huang, and T. E. Yankeelov, "Incorporating drug delivery into an imaging-driven, mechanics-coupled reaction diffusion model for predicting the response of breast cancer to neoadjuvant chemotherapy: theory and preliminary clinical results," *Physics in Medicine & Biology*, vol. 63, no. 10, p. 105015, 2018. (doi:10.1088/1361-6560/aac040).
18. T. E. Yankeelov, M. Lepage, A. Chakravarthy, E. E. Broome, K. J. Niermann, M. C. Kelley, I. Meszoely, I. A. Mayer, C. R. Herman, K. McManus, *et al.*, "Integration of quantitative dce-mri and adc mapping to monitor treatment response in human breast cancer: initial results," *Magnetic resonance imaging*, vol. 25, no. 1, pp. 1–13, 2007. (doi:10.1016/j.mri.2006.09.006).
19. K. R. Swanson, R. C. Rockne, J. Claridge, M. A. Chaplain, E. C. Alvord, and A. R. Anderson, "Quantifying the role of angiogenesis in malignant progression of gliomas: in silico modeling integrates imaging and histology," *Cancer research*, vol. 71, no. 24, pp. 7366–7375, 2011. (doi:10.1158/0008-5472.CAN-11-1399).
20. D. A. Hormuth, J. A. Weis, S. L. Barnes, M. I. Miga, E. C. Rericha, V. Quaranta, and T. E. Yankeelov, "A mechanically coupled reaction–diffusion model that incorporates intra-tumoural heterogeneity to predict in vivo glioma growth," *Journal of The Royal Society Interface*, vol. 14, no. 128, p. 20161010, 2017. (doi:10.1098/rsif.2016.1010).
21. S. Gu, G. Chakraborty, K. Champley, A. M. Alessio, J. Claridge, R. Rockne, M. Muzi, K. A. Krohn, A. M. Spence, E. C. Alvord, *et al.*, "Applying a patient-specific bio-mathematical model of glioma growth to develop virtual [18f]-fmiso-pet images," *Mathematical Medicine and Biology*, vol. 29, no. 1, pp. 31–48, 2012. (doi:10.1093/imammb/dqr002).
22. A. Hawkins-Daarud, R. C. Rockne, A. R. Anderson, and K. R. Swanson, "Modeling tumor-associated edema in gliomas during anti-angiogenic therapy and its impact on imageable tumor," *Frontiers in oncology*, vol. 3, p. 66, 2013. (doi:10.3389/fonc.2013.00066).
23. A. Martínez-González, G. F. Calvo, L. A. P. Romasanta, and V. M. Pérez-García, "Hypoxic cell waves around necrotic cores in glioblastoma: a biomathematical model and its therapeutic implications," *Bulletin of mathematical biology*, vol. 74, no. 12, pp. 2875–2896, 2012. (doi:10.1007/s11538-012-9786-1).
24. V. M. Pérez-García and L. A. Pérez-Romasanta, "Extreme protraction for low-grade gliomas: theoretical proof of concept of a novel therapeutical strategy," *Mathematical Medicine and*

Biology, pp. 253–271, 2015.
(doi:10.1093/imammb/dqv017).

25. R. C. Rockne, A. D. Trister, J. Jacobs, A. J. Hawkins-Daarud, M. L. Neal, K. Hendrickson, M. M. Mrugala, J. K. Rockhill, P. Kinahan, K. A. Krohn, *et al.*, "A patient-specific computational model of hypoxia-modulated radiation resistance in glioblastoma using 18f-fmiso-pet," *Journal of the Royal Society Interface*, vol. 12, no. 103, p. 20141174, 2015.
(doi:10.1098/rsif.2014.1174).
26. J. A. Weis, M. I. Miga, and T. E. Yankeelov, "Three-dimensional image-based mechanical modeling for predicting the response of breast cancer to neoadjuvant therapy," *Computer methods in applied mechanics and engineering*, vol. 314, pp. 494–512, 2017.
(doi:10.1016/j.cma.2016.08.024).
27. T. E. Yankeelov, N. Atuegwu, D. Hormuth, J. A. Weis, S. L. Barnes, M. I. Miga, E. C. Rericha, and V. Quaranta, "Clinically relevant modeling of tumor growth and treatment response," *Science translational medicine*, vol. 5, no. 187, pp. 187ps9–187ps9, 2013.
(doi:10.1126/scitranslmed.3005686).
28. C. Johnson, *Numerical solution of partial differential equations by the finite element method*.
Courier Corporation, 2012.
29. G. Strang, *Introduction to applied mathematics*, vol. 16.
Wellesley-Cambridge Press Wellesley, MA, 1986.
30. H. Gomez, M. Bures, and A. Moure, "A review on computational modelling of phase-transition problems," *Philosophical Transactions of the Royal Society A*, vol. 377, no. 2143, p. 20180203, 2019.
(doi:10.1098/rsta.2018.0203).
31. P. Colli, H. Gomez, G. Lorenzo, G. Marinoschi, A. Reali, and E. Rocca, "Mathematical analysis and simulation study of a phase-field model of prostate cancer growth with chemotherapy and antiangiogenic therapy effects," *arXiv preprint arXiv:1907.11618*, 2019.